Volume 7 | Number 7 | July 2014 | Pages 2045–2384

Energy & Environmental Science

www.rsc.org/ees

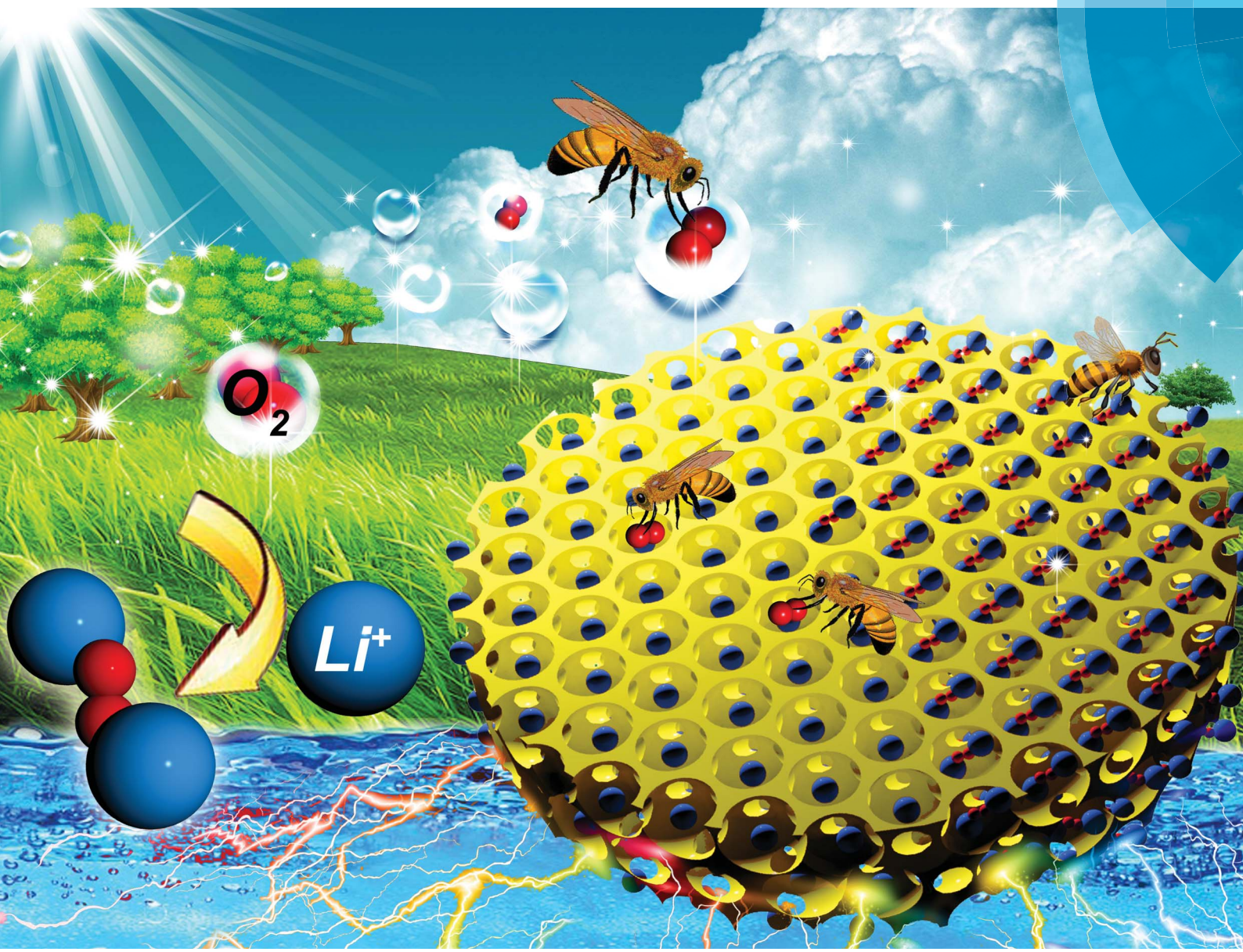

ISSN 1754-5692

ROYAL SOCIETY OF CHEMISTRY

COMMUNICATION

Xin-Bo Zhang *et al.*

3D ordered macroporous $LaFeO_3$ as efficient electrocatalyst for Li–O_2 batteries with enhanced rate capability and cyclic performance

Energy & Environmental Science

COMMUNICATION

View Article Online
View Journal | View Issue

Cite this: *Energy Environ. Sci.*, 2014, 7, 2213

Received 30th August 2013
Accepted 25th November 2013

DOI: 10.1039/c3ee42934b

www.rsc.org/ees

3D ordered macroporous $LaFeO_3$ as efficient electrocatalyst for Li–O_2 batteries with enhanced rate capability and cyclic performance†

Ji-Jing Xu, Zhong-Li Wang, Dan Xu, Fan-Zhi Meng and Xin-Bo Zhang*

Rechargeable lithium–oxygen (Li–O_2) battery is one of the most promising technologies among various electrochemical energy storage systems, while the incapability of the electrocatalyst and the inefficient transport of reactants in the O_2 electrode still limit the round-trip efficiency, rate capability, and cycle stability of the Li–O_2 battery. Here, three-dimensional ordered macroporous $LaFeO_3$ (3DOM-LFO) is synthesized and employed as electrocatalyst in Li–O_2 battery with relatively stable TEGDME based electrolyte. The Li–O_2 cells with 3DOM-LFO show enhanced electrochemical performances, including low overpotential, high specific capacity, good rate capability and cycle stability up to 124 cycles. This enhanced catalytic performance might be due to the synergistic effect of the porosity and catalytic activity of the 3DOM-LFO catalyst.

Broader context

Rechargeable Li–O_2 batteries hold much higher energy density than that can be achieved by the best of Li-ion batteries, which is thus of great importance for large scale electricity energy storage. Up to now, Li–O_2 batteries are still facing many challenges including low energy efficiency, poor rate capability, and short cycle life, which are partially limited by the sluggish kinetics of ORR and OER processes. Therefore, developing of highly efficient electrocatalyst is of great importance. In our current work, three-dimensional ordered macroporous $LaFeO_3$ is synthesized through a template replication approach. When first employed as electrocatalyst for rechargeable Li–O_2 batteries, enhanced electrochemical performances including rate capability and cycle stability are obtained, which could promote the development of advanced Li–O_2 batteries. The application of $LaFeO_3$ synthesized with low cost could be easily extended to other energy storage/conversion systems like fuel cells.

Introduction

Rechargeable lithium–oxygen (Li–O_2) batteries have recently attracted a great deal of attention because they can theoretically provide much higher energy than current lithium-ion batteries, which is vital for electric vehicles, future renewable energy storage, and other high energy applications.[1–6] However, to enable Li–O_2 batteries for practical applications, numerous scientific challenges need to be overcome, including poor rate capability, low round-trip efficiency (due to bad overpotentials for both oxygen reduction and evolution), instability of electrolyte, and especially short cycle life.[7–10] In response, previous studies have reported that these limitations can be partially overcome by protecting the electrolyte and lithium anode and/or employing a sophisticated cathode and effective electrocatalyst. For example, a number of studies have demonstrated that the use of stable solid electrolytes can improve large polarization and overcome electrolyte decomposition in the cell using organic liquid electrolytes. In addition, using dense solid electrolyte also has the advantage that the lithium anode can be protected from corrosion by vapor water, oxygen, nitrogen and carbon dioxide in ambient air.[11,12] Our previous studies demonstrate that employing a sophisticated cathode and effective electrocatalyst could accelerate the kinetic reactions and thus improve the overall energy storage efficiency, which is consistent with the results obtained by other groups.[5,13–16] Earlier investigations of cathode catalysts including metal oxide, metal nitride, metal nanoparticles, and organometallic compounds, *etc.*, were conducted in Li–O_2 battery with carbonate electrolyte.[17–27] Recently, many electrocatalysts including bismuth and lead ruthenate pyrochlores, metallic mesoporous pyrochlore catalyst, Co_3O_4 grown on reduced grapheme oxide, Fe/N/C composite, hydrate ruthenium oxide, and Pd nanoparticles were reported in Li–O_2 cells with a glyme-based electrolyte and showed high reversible capacity with a lower charge potential for OER than pure carbon.[28–33] On the other hand, precipitation of insoluble and insulate discharge products in the O_2 electrode would gradually block the electrolyte, oxygen and electron pathway and eventually limit the rate capability, capacity, and cyclic life of the Li–O_2 batteries.[34]

State Key Laboratory of Rare Earth Resource Utilization, Changchun Institute of Applied Chemistry, Chinese Academy of Sciences, Changchun 130022, China. E-mail: xbzhang@ciac.ac.cn; Fax: +86-431-85262235; Tel: +86-431-85262235

† Electronic supplementary information (ESI) available. See DOI: 10.1039/c3ee42934b

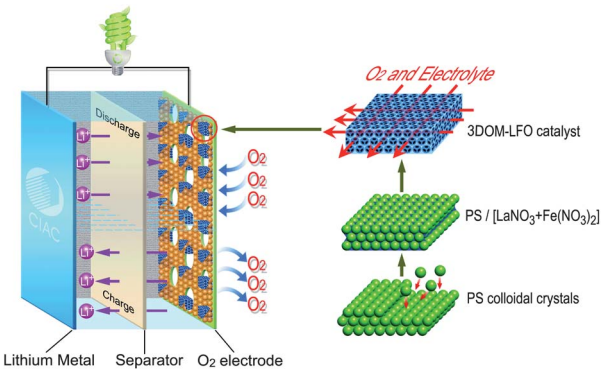

Fig. 1 Schematic illustration for preparation of 3DOM-LFO catalyst and structure of the rechargeable Li–O_2 batteries.

Therefore, development of well-ordered porous O_2 electrode catalysts to efficiently catalyze Li–O_2 reactions in relatively stable ether-based electrolytes, while simultaneously facilitating rapid oxygen and electrolyte diffusion, is highly desirable yet still very challenging.

Perovskite-based oxides, as one of the most important families of functional inorganic materials, hold many favorable physical/chemical properties, including high electronic/ionic conductivity, high electrochemical stability, and enhanced catalytic characteristics,[35] and thus could be employed as electrocatalyst for Li–O_2 batteries.[14,36–38] Herein, we report a rational and facile strategy for preparing three-dimensionally ordered macroporous $LaFeO_3$ (3DOM-LFO). When it is employed as the O_2 electrode catalyst (Fig. 1), the Li–O_2 cells show an enhanced specific capacity, rate capability, and cycle stability.

Experimental procedure

Polystyrene sphere template preparation

Monodispersed polystyrene sphere (PS) dispersions were prepared by emulsion polymerization using styrene (CP), sodium dodecyl sulfate (SDS), potassium persulfate (KPS), and anhydrous alcohol. Then, the PS spheres were close-packed into colloidal crystals by centrifugation (2000 rpm, 20 h) followed by drying at 60 °C for 8 h. These dried samples were used as templates in the synthesis of three-dimensionally ordered macroporous $LaFeO_3$ catalyst.

Preparation of 3DOM-LFO and LFO nanoparticles

Precursor solutions were obtained by dissolving a desired amount of mixed metal salt [$LaNO_3 \cdot 6H_2O : Fe(NO_3)_3 \cdot 9H_2O$ = 1 : 1] into an ethylene glycol (EG)-methanol (30–50 vol%) mixed solvent at room temperature. Then, the PS colloidal crystals were soaked in the metal precursor solution for 1 h, and the excess solution was removed from the impregnated PS template by filtration. The obtained sample was allowed to dry in air at 60 °C for 2 h. The polystyrene spheres were removed by calcining in flowing air at a temperature of 400 °C. The temperature heating rate is 1 °C min^{-1}. Then the sample was heated in a muffle furnace under different calcination conditions. LFO nanoparticles (LFO-NP) were prepared using the same procedure except without PS template.

Characterizations

The morphologies and structures of 3DOM-LFO and NP-LFO catalysts were characterized using various physiochemical techniques, including powder X-ray diffraction (XRD), field emission scanning electron microscopy (FESEM), transmission electron microscopy (TEM), and nitrogen adsorption/desorption isotherms.

Li–O_2 cell preparation and electrochemical performance measurements

The electrochemical performance of Li–O_2 cells was carried out using 2025-type coin cell. All cells were assembled in glove box under Ar atmosphere, using a lithium metal foil anode, glass fibre separator, oxygen cathode, and electrolyte containing 1 M LITFSI in TEGDME (Fig. 1). The O_2 electrodes were prepared by coating homogenous ink composed of a mixture of 30 wt% 3DOM-LFO or NP-LFO catalyst, 60 wt% KB, 10 wt% lithiated Nafion onto a nickel foam current collector. Assuming complete oxidation, the artificially Li_2O_2-loaded electrode has a calculated capacity of 2000 mA h g_{carbon}^{-1}. The galvanostatic discharge/charge tests were conducted within a voltage window of 2.2–4.4 V (*vs.* Li/Li^+) at ambient temperature. To avoid complications related to H_2O and CO_2 contamination, the cells were operated at 1 atm of pure O_2. All specific capacity results were calculated with the mass of the carbon in O_2 electrodes. Electrochemical impedance spectroscopy of the cells was evaluated using an electrochemical workstation within a frequency range of 8×10^8 to 10^{-2} Hz. A three-electrode cell for RDE (rotating disk electrode) measurements containing 1 M LiTFSI in TEGDME electrolyte was assembled in a dry argon-filled glove box. The Ag/Ag^+ reference electrode consisted of a Ag wire immersed into 0.1 M $TBAPF_6$ and 0.01 M $AgNO_3$ in TEGDME solution and was connected to the main compartment by a Vycor frit.[39] All potentials reported in this work, however, are referenced to the Li/Li^+ potential, and obtained by calibration of the reference electrode against a fresh lithium foil in a 1 M LiTFSI solution in TEGDME before the experiments. Cyclic voltammograms (CVs) were recorded between 1.7 and 4.5 V (*vs.* Li/Li^+) at a voltage sweep rate of 10 mV s^{-1} and a rotating rate of 900 rpm.

Results and discussion

As shown in Fig. 1, the 3DOM-LFO is prepared by a facile but efficient colloidal crystal template method. The field emission scanning electron microscopy (FESEM) and transmission electron microscopy (TEM) images (Fig. 2a–c) clearly show that the close packing order of the original polystyrene template (Fig. S1a†) is successfully preserved even after the calcined process at 600 °C for 3 h. Well-ordered "air spheres" and interconnected inorganic walls create a "honeycomb" pore structure in three dimensions. Naturally, the open and interconnected 3DOM structure could give a high specific area to

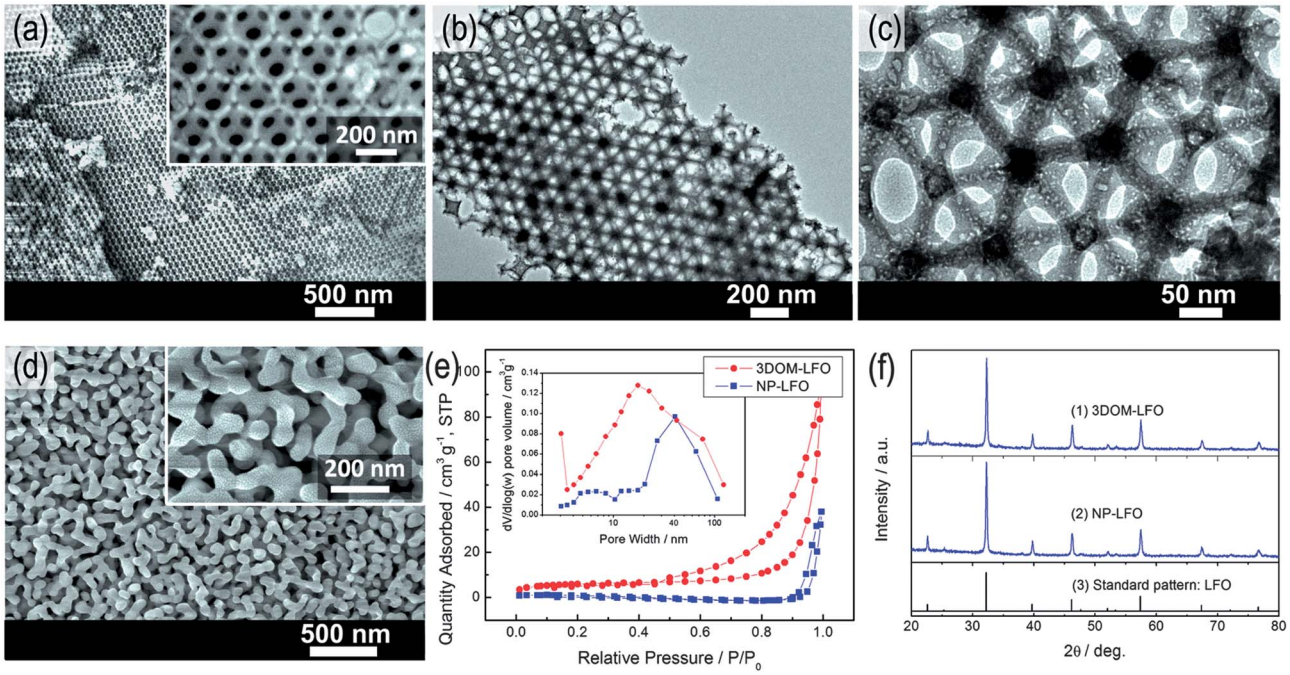

Fig. 2 (a) FESEM images of 3DOM-LFO after calcination at 600 °C for 3 h. Inset in (a): magnified FESEM image. (b) Low-resolution and (c) higher-resolution TEM images of 3DOM-LFO catalyst. (d) FESEM images of NP-LFO after calcination at 600 °C for 3 h. Inset in (d): magnified FESEM image. (e) Nitrogen adsorption–desorption isotherms and pore size distribution of 3DOM-LFO. (f) X-Ray diffraction patterns of 3DOM-LFO and NP-LFO catalysts.

expose more surface sites. This is further proved by the N_2 absorption–desorption isotherms of 3DOM-LFO (Fig. 2e). The sample is found to shows a IV type N_2 absorption–desorption isotherm, which is characteristic of a mesoporous material.[40] Brunauer–Emmett–Teller (BET) measurement shows that the surface area of the prepared 3DOM-LFO is 29.3 $m^2\ g^{-1}$. This favourable well-ordered pore structure of 3DOM-LSM would certainly facilitate the diffusion of oxygen and electrolyte in O_2 electrode, ensure high availability of the catalytic active sites, and thus certainly benefit the electrochemical performance of Li–O_2 batteries (*vide infra*). For comparison, nonporous $LaFeO_3$ nanoparticles (NP-LFO) are also synthesized. The particle size is found to be *ca.* 50 nm (Fig. 2d) and the BET surface area is calculated to be about 1.4 $m^2\ g^{-1}$. The powder X-ray diffraction (XRD) patterns of the 3DOM- and NP-LFO are shown in Fig. 2f. All diffraction peaks can be ascribed to the well-crystallized $LaFeO_3$ (PDF no. 37-1493) without any impure phases.

The electrocatalytic activity of 3DOM-LFO catalyst for ORR and OER is then examined in Li–O_2 cells and compared to NP-LFO and Ketjenblack carbon (KB). The first discharge/charge profiles of Li–O_2 cells with the three different O_2 electrodes are displayed in Fig. 3a. Interestingly, it can be found that the discharge and especially the charge voltage of Li–O_2 cells can be improved with the help of the 3DOM-LFO catalyst, which would consequently enhance round-trip efficiency. In detail, although the discharge voltage of Li–O_2 cells with 3DOM-LFO/KB electrode is only slightly higher than that of NP-LFO/KB by about 20 mV and KB by about 30 mV, its charge voltage is much lower than that of Li–O_2 cells with NP-LFO/KB electrode by 150 mV and KB by 250 mV. In order to avoid complications from possible electrolyte decomposition during a prolonged discharge reaction, the three artificially Li_2O_2-loaded electrodes are also subjected to electrochemical oxidation in Li–O_2 cells, as shown in Fig. S4.† It can be seen that a similar reduction in the charge voltage of about 130 and 210 mV is obtained for the oxidation of Li_2O_2 on 3DOM-LFO/KB electrode *versus* NP-LFO/KB and KB, as observed in the charge profile shown in Fig. 3a. It should be noted that the differences in charge voltage between true discharged and artificially "discharged" electrodes might be due to the different forms of Li_2O_2 on electrodes. The CV (Fig. 3b) is then used to further compare the ORR and OER in 1 M LITFSI in TEGDME electrolyte. Compared with the KB electrode, the 3DOM-LFO-based electrode exhibits a higher ORR onset potential and ORR/OER peak current. The enhanced ORR/OER kinetics could lead to improvements in the energy output, the recharging characteristic, and the round-trip efficiency of the Li–O_2 cell.

Inspired by the power of 3DOM-LFO electrocatalyst in suppressing the overpotentials, we then further examine its efficacy on the rate performance of Li–O_2 cells. It can be seen that the Li–O_2 cells with 3DOM-LFO/KB electrode exerts a higher discharge capacity (Fig. 3c) and capacity retention capability (Fig. 3d) than those with NP-LFO/KB and pure KB electrodes under all investigated current densities (0.025 to 0.2 mA cm^{-2}). This enhanced rate property could be reasonably attributed to the synergistic effect of the catalytic activity and porosity of the 3DOM-LFO catalyst. This can be further clarified by the morphology of the 3DOM-LFO/KB electrode (Fig. 4a). Clearly, in

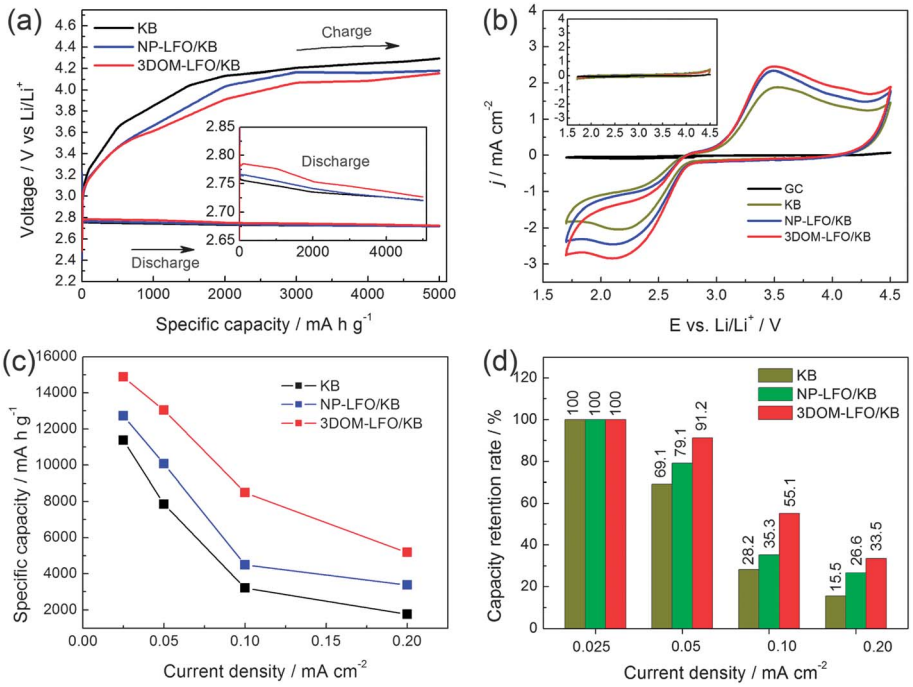

Fig. 3 (a) First charge–discharge curves of Li–O_2 cells with pure KB, NP-LFO/KB, and 3DOM-LFO/KB electrodes at a current density of 0.025 mA cm^{-2}. Inset from (a): discharge voltages of Li–O_2 cells. (b) CVs of glassy carbon (GC), NP-LFO/KB, 3DOM-LFO/KB, and KB alone on GC recorded in O_2-saturated electrolyte containing 1 M LiTFSI in TEGDME at a voltage sweep rate of 10 mV s^{-1} and rotating rate of 900 rpm. Inset: CVs in Ar-saturated electrolyte, showing no activity. Comparison of (c) discharge specific capacity and (d) capacity retention capability of Li–O_2 cells with the three kinds of O_2 electrodes at different current densities.

a 3DOM-LFO/KB electrode, the unique "honeycomb" porous structure unit of 3DOM-LFO is embedded inside KB carbon, leading to a favourable three-dimensional frame electrode structure which can thus provide a sufficient void volume for Li_2O_2 deposition, resulting in higher discharge capacity. In addition, this 3D porous structure would offer more abundant oxygen and electrolyte transportation paths, helping to get uniform O_2 and electrolyte distribution inside the electrode, which is supposed to be beneficial for the rate capability of Li–O_2 cells.[41,42] Furthermore, to exclude possible electrochemical contributions from lithium ions (Li^+) intercalation into carbon or perovskite-based oxide materials, the initial discharge curves of Li–O_2 cells with pure KB NP-LFO/KB, and 3DOM-LFO/KB cathodes in argon (Ar) atmosphere are also tested for comparison (Fig. S6†). Clearly, the background discharge capacity is negligible within the voltage range, which suggests that the above obtained enhanced discharge capacities of Li–O_2 cells are derived from the oxygen reduction.

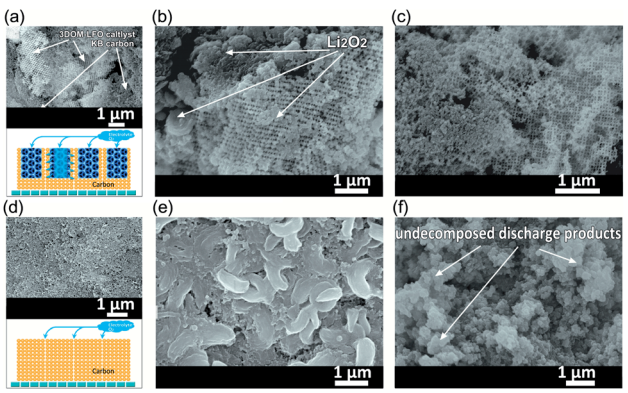

Fig. 4 FESEM images of 3DOM-LFO/KB electrode (a) before discharge, (b) in the discharge state and (c) in the reverse charged state. FESEM images of a pure KB electrode (d) before discharge, (e) in the discharge state and (f) in the reverse charged state. Current density: 0.05 mA cm^{-2}.

We further examined the cycling performances of the Li–O_2 cells with the three kinds of O_2 electrodes (Fig. 5). The Li–O_2 cells with 3DOM-LFO catalyst present better cycle stability than those with NP-LFO and pure KB. The Li–O_2 cells with 3DOM-LFO holds the capacity of 11738 mA h g^{-1} during the initial discharge and a high value of 11932 mA h g^{-1} is still obtained after four cycles (Fig. 5c); while with KB alone electrode, the discharge capacity decreased dramatically upon cycling and down to 2571 mA h g^{-1} after four cycles (Fig. 5a). This enhanced cycling stability could be attributed to the unique properties of the O_2 electrode with well-ordered porous 3DOM-LFO electrocatalyst, which facilitate the formation and decomposition of the product and thus improved the rechargeability of the O_2 electrode. To clarify this point, the morphological changes of O_2 electrodes after discharge and charge for pure KB and 3DOM-LFO/KB electrodes are examined (Fig. 4b, c, e, and f). It is found that, after discharge, the surface of KB electrode almost fully adhered to a film (Fig. 4e), which would inevitably impede lithium-ion and charge transfer within the electrode during

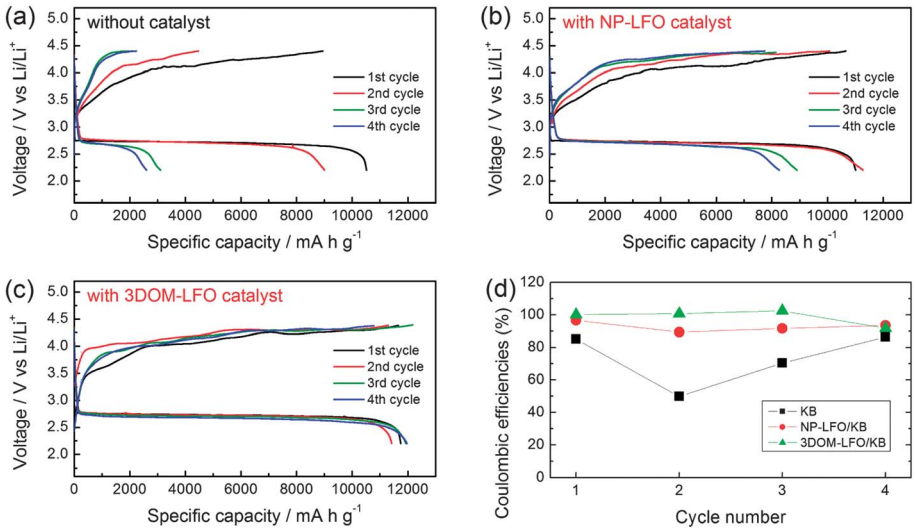

Fig. 5 Cyclic performance of Li–O_2 cells with (a) pure KB, (b) NP-LFO/KB, and (c) 3DOM-LFO/KB electrodes at a current density of 0.025 mA cm^{-2}. (d) Comparison of coulombic efficiency of Li–O_2 cells with the three kinds of electrodes.

subsequent cycling, and thus the rechargeability of the pure KB electrode is very poor. In contrast, after discharge, the 3DOM-LFO/KB electrode retained its porous structure and morphology, without the formation of a thick coating layer (Fig. 4b), ensuring uniform oxygen and electrolyte distribution around the discharge products, which can thus promote the decomposition of the products, facilitate recovery of the electrode porosity during charge (Fig. 4c) and result in enhancement of rechargeability on 3DOM-LFO/KB electrode.

Fig. 5d depicts the discharge/charge specific capacity and coulombic efficiency of the Li–O_2 cells with 3DOM-LFO/KB and pure KB electrodes at a current density of 0.025 mA cm^{-2}. It is observed that the charge capacity is close to the discharge capacity on each cycle for Li–O_2 cells with 3DOM-LFO/KB electrode, which demonstrates that the 3DOM-LFO/KB electrode holds an enhanced charging efficiency. On the contrary, the average coulombic efficiency of the KB electrode is only *ca.* 75%. These results indicate that the 3DOM-LFO electrocatalyst can also improve the charge efficiency of Li–O_2 cells. In order to more clearly describe the details of the differences in charge efficiencies of the electrodes, the electrochemical impedance spectra (EIS) of both Li–O_2 cells at different discharge/charge stages are tested. As shown in Fig. 6, it is found that the impedances of both Li–O_2 cells before first discharge are almost the same. After the first discharge, the impedances of both cells increase significantly, which is due to the poor electronic conductive discharge products (Li_2O_2) generated in the O_2 electrode. Interestingly, after the charging process, Li–O_2 cells with 3DOM-LFO catalyst can almost recover the impedances (Fig. 6a), indicating that the formed insulated product can be almost fully decomposed upon charging, which is consistent with the SEM images of the 3DOM-LFO electrode after charging (Fig. 4c). On the contrary, the impedance of Li–O_2 cells with KB alone electrode increases monotonously along the discharge/charge processes (Fig. 6b) due to incomplete decomposition of the discharge products (Fig. 4f), highlighting again the unique properties of the electrode with 3DOM-LFO electrocatalyst.

The results above demonstrate the enhanced performance of 3DOM-LFO electrocatalyst for Li–O_2 batteries. To further verify its universality, we then extend the battery test to other

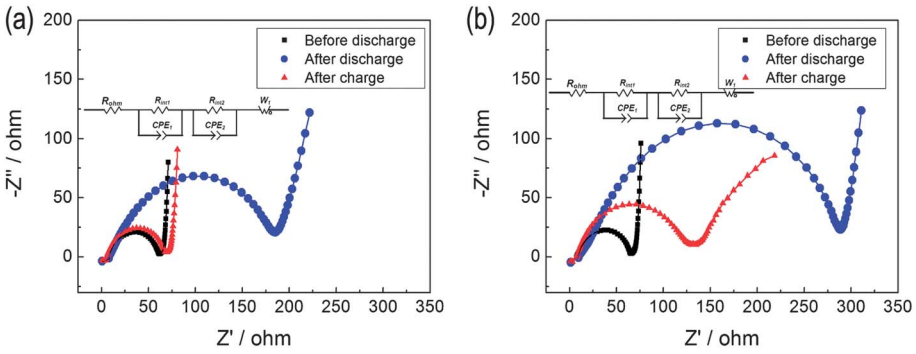

Fig. 6 Electrochemical impedance spectra of Li–O_2 cells (a) with or (b) without 3DOM-LFO catalyst at different discharge/charge stages (current density: 0.05 mA cm^{-2}).

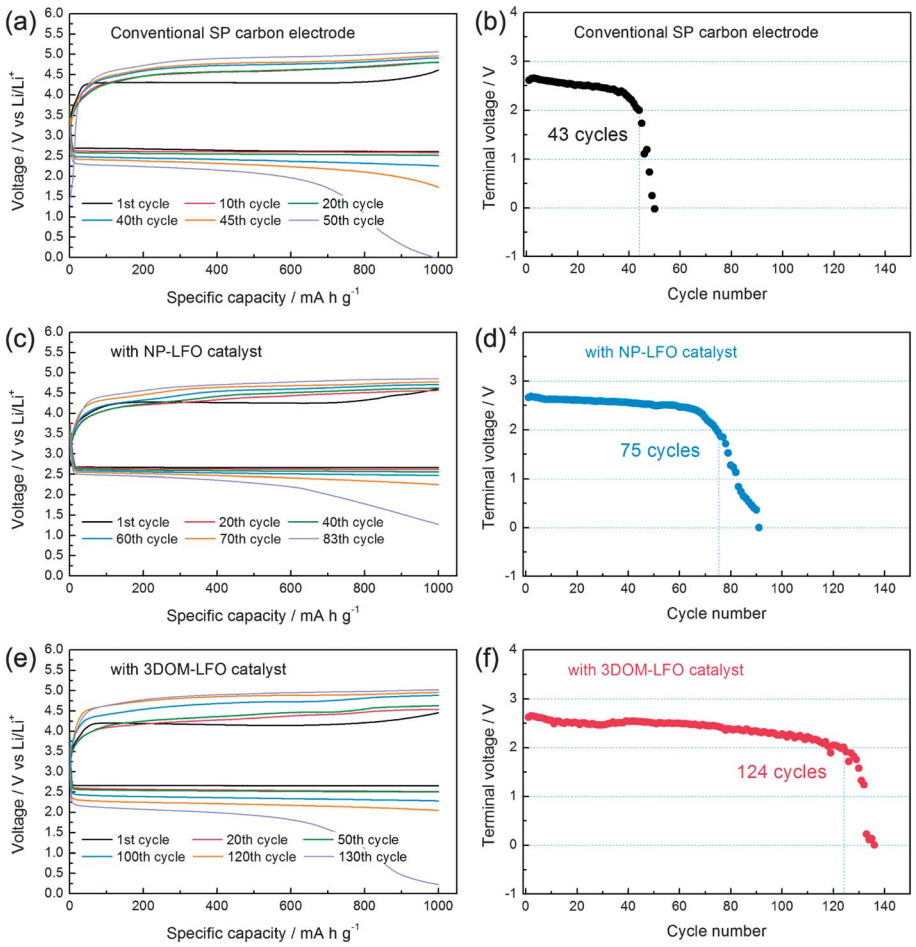

Fig. 7 Cycling response of the Li–O_2 cells with (a and b) Super P carbon (SP), (c and d) NP-LFO/SP, and (e and f) 3DOM-LFO/SP electrodes under a specific capacity limit of 1000 mA h g_{carbon}^{-1}. Current density: 0.15 mA cm^{-2}. (a, c and e) Discharge/charge curves at different cycles; (b, d and f) voltage on the terminal of discharge *vs.* cycle number.

electrode systems by employing another commonly used carbon, commercial Super P carbon (SP), as electrode support material for Li–O_2 batteries. There is almost no degradation of Li–O_2 cells with 3DOM-LFO/SP electrode even after 124 cycles (Fig. 7e and f). On the contrary, the operations of Li–O_2 cells are limited to 43 or 75 cycles for Li–O_2 batteries without catalyst (Fig. 7a and b) or with NP-LFO catalyst (Fig. 7c and d). These results highlight again the power of 3DOM-LFO electrocatalyst and indicate that we can further improve the performance of Li–O_2 batteries by choosing a suitable stable electrolyte and appropriate cell design.

Conclusions

In summary, 3DOM-LFO is prepared by a rational and facile strategy. When employed as a catalyst in rechargeable Li–O_2 batteries, the 3DOM-LFO suppresses the ORR and especially OER overpotentials in ether-based electrolytes. Furthermore, the improved Li–O_2 cells exhibit enhanced specific capacity, rate capacity, and cycling performance, which is considered to stem from the synergistic effect of catalytic activity and porosity of the 3DOM-LFO catalyst. In addition, recent research shows that further improvement in cycling life (in air), specific capacity, and overpotentials could be achieved by fine tuning of the electrolyte and/or air cathode.[2,43,44] This significant progress would lead to improved strategies for advanced rechargeable Li–air batteries.

Acknowledgements

This work is financially supported by 100 Talents Programme of The Chinese Academy of Sciences, National Program on Key Basic Research Project of China (973 Program, Grant no. 2014CB932300, 2012CB215500), Foundation for Innovative Research Groups of the National Natural Science Foundation of China (Grant no. 20921002), National Natural Science Foundation of China (Grant no. 21101147 and 21203176).

Notes and references

1 M. Leskes, N. E. Drewett, L. J. Hardwick, P. G. Bruce, G. R. Goward and C. P. Grey, *Angew. Chem., Int. Ed.*, 2012, **51**, 8560–8563.
2 T. Zhang and H. S. Zhou, *Nat. commun.*, 2013, **4**, 2855.

3 Y. C. Lu, H. A. Gasteiger and Y. Shao-Horn, *J. Am. Chem. Soc.*, 2011, **133**, 19048–19051.
4 Y. G. Wang and H. S. Zhou, *Energy Environ. Sci.*, 2011, **4**, 1704–1707.
5 J.-J. Xu, Z.-L. Wang, D. Xu, L.-L. Zhang and X.-B. Zhang, *Nat. commun.*, 2013, **4**, 2438.
6 Z. Q Peng, S. A. Freunberger, Y. H. Chen and P. G. Bruce, *Science*, 2012, **337**, 563–566.
7 G. Girishkumar, B. McCloskey, A. C. Luntz, S. Swanson and W. Wilcke, *J. Phys. Chem. Lett.*, 2010, **1**, 2193–2203.
8 (*a*) P. G. Bruce, S. A. Freunberger, L. J. Hardwick and J.-M. Tarascon, *Nat. Mater.*, 2012, **11**, 19–29; (*b*) W. Walker, V. Giordani, J. Uddin, V. S. Bryantsev, G. V. Chase and D. Addison, *J. Am. Chem. Soc.*, 2013, **135**, 2076–2079; (*c*) Y. L. Li, X. F. Li, D. S. Geng, Y. J. Tang, R. Y. Li, J.-P. Dodelet, M. Lefévre and X. L. Sun, *Carbon*, 2013, **64**, 170–177; (*d*) Y. L. Li, J. J. Wang, X. F. Li, D. S. Geng, M. N. Banis, R. Y. Li and X. L. Sun, *Electrochem. Commun.*, 2012, **18**, 12–15.
9 K. M. Abraham and Z. Jiang, *J. Electrochem. Soc.*, 1996, **143**, 1–5.
10 D. Zhai, H.-H. Wang, J. Yang, K. C. Lau, K. Li, K. Amine and L. A. Curtiss, *J. Am. Chem. Soc.*, 2013, **135**, 15364–15372.
11 H. Kitaura and H. S. Zhou, *Energy Environ. Sci.*, 2012, **5**, 9077–9084.
12 P. Kichambare, S. Rodrigues and J. Kumar, *ACS Appl. Mater. Interfaces*, 2012, **4**, 49–52.
13 J. J. Wang, Y. L. Li and X. L. Sun, *Nano Energy*, 2013, **2**, 443–467.
14 J.-J. Xu, D. Xu, Z.-L. Wang, H.-G. Wang, L.-L. Zhang and X.-B. Zhang, *Angew. Chem., Int. Ed.*, 2013, **52**, 3887–3890.
15 Z.-L. Wang, D. Xu, J.-J. Xu, L.-L. Zhang and X.-B. Zhang, *Adv. Funct. Mater.*, 2012, **22**, 3699–3705.
16 M. M. O. Thotiyl, S. A. Freunberger, Z. Peng, Y. Chen, Z. Liu and P. G. Bruce, *Nat. Mater.*, 2013, **12**, 1050–1056.
17 A. Débart, A. J. Paterson, J. Bao and P. G. Bruce, *Angew. Chem.*, 2008, **47**, 4597–4600.
18 F. Cheng, J. Shen, W. Ji, Z. Tao and J. Chen, *ACS Appl. Mater. Interfaces*, 2009, **1**, 460–466.
19 A. K. Thapa and T. Ishihara, *J. Power Sources*, 2011, **196**, 7016–7020.
20 A. Débart, J. Bao, G. Armstrong and P. G. Bruce, *J. Power Sources*, 2007, **174**, 1177–1182.
21 Y. M. Cui, Z. Y. Wen and Y. Liu, *Energy Environ. Sci.*, 2011, **4**, 4727–4734.
22 H. L. Wang, Y. Yang, Y. Y. Liang, G. Y. Zheng, Y. G. Li, Y. Cui and H. J. Dai, *Energy Environ. Sci.*, 2012, **5**, 7931–7935.
23 S. M. Dong, X. Chen, K. J. Zhang, L. Gu, L. X. Zhang, X. H. Zhou, L. F. Li, Z. H. Liu, P. X. Han, H. X. Xu, J. H. Yao, C. J. Zhang, X. Y. Zhang, C. Q. Shang, G. L. Cui and L. Q. Chen, *Chem. Commun.*, 2011, **47**, 11291–11293.
24 Y. C. Lu, Z. Xu, H. A. Gasteiger, S. Chen, K. Hamad-Schifferli and Y. Shao-Horn, *J. Am. Chem. Soc.*, 2010, **132**, 12170–12171.
25 Y. C. Lu, D. G. Kwabi, K. P. C. Yao, J. R. Harding, J. Zhou, L. Zuind and Y. Shao-Horn, *Energy Environ. Sci.*, 2011, **4**, 2999–3007.
26 X. M. Ren, S. S. Zhang, D. T. Tran and J. Read, *J. Mater. Chem.*, 2011, **21**, 10118–10125.
27 Y. Cao, Z. Wei, J. He, J. Zang, Q. Zhang, M. Zheng and Q. Dong, *Energy Environ. Sci.*, 2012, **5**, 9765–9768.
28 S. H. Oh and L. F. Nazar, *Adv. Energy Mater.*, 2012, **2**, 903–910.
29 S. H. Oh, R. Black, E. Pomerantseva, J. H. Lee and L. F. Nazar, *Nat. Chem.*, 2012, **4**, 1004–1010.
30 R. Black, J. H. Lee, B. Adams, C. A. Mims and L. F. Nazar, *Angew. Chem., Int. Ed.*, 2012, **51**, 1–6.
31 J. Shui, N. K. Karan, M. Balasubramanian, S. Lic and D. J. Liu, *J. Am. Chem. Soc.*, 2012, **134**, 16654–16661.
32 H.-G. Jung, Y. S. Jeong, J.-B. Park, Y.-K. Sun, B. Scrosati and Y. J. Lee, *ACS Nano*, 2013, **7**, 3532–3539.
33 J. Lu, Y. Lei, K. C. Lau, X. Luo, P. Du, J. Wen, R. S. Assary, U. Das, D. J. Miller, J. W. Elam, H. M. Albishri, D. A. El-Hady, Y.-K. Sun, L. A. Curtiss and K. Amine, *Nat. Commun.*, 2013, **4**, 3383.
34 T. Zhang and H. S. Zhou, *Angew. Chem.*, 2012, **124**, 11224–11229.
35 J. Suntivich, H. A. Gasteiger, N. Yabuuchi, H. Nakanishi, J. B. Goodenough and Y. Shao-Horn, *Nat. Chem.*, 2011, **3**, 546–550.
36 Y. L. Zhao, L. Xu, L. Q. Mai, C. H. Han, Q. Y. An, X. Xu, X. Liu and Q. J. Zhang, *Proc. Natl. Acad. Sci. U. S. A.*, 2012, **109**, 19569–19574.
37 Z. H. Fu, X. J. Lin, T. Huang and A. S. Yu, *J. Solid State Electrochem.*, 2012, **16**, 1447–1452.
38 W. Yang, J. Salim, S. Li, C. Sun, L. Chen, J. B. Goodenough and Y. Kim, *J. Mater. Chem.*, 2012, **22**, 18902–18907.
39 Y. C. Lu, H. A. Gasteiger, E. Crumlin, R. McGuire Jr and Y. Shao-Horn, *J. Electrochem. Soc.*, 2010, **157**, A1016–A1025.
40 K. S. W. Sing, D. H. Everett, R. A. W. Haul, L. Moscou, R. A. Pierotti, J. Rouquerol and T. Siemieniewska, *Pure Appl. Chem.*, 1985, **57**, 603–619.
41 Y. M. Cui, Z. Y. Wen, X. Liang, Y. Lu, J. Jin, M. F. Wu and W. Wu, *Energy Environ. Sci.*, 2012, **5**, 7893–7897.
42 Y. L. Li, J. J. Wang, X. F. Li, D. S. Geng, M. N. Banis, Y. J. Tang, D. G. Wang, R. Y. Li, T.-K. Sham and X. L. Sun, *J. Mater. Chem.*, 2012, **22**, 20170–20174.
43 J. Xiao, D. Mei, X. Li, W. Xu, D. Wang, G. L. Graff, W. D. Bennett, Z. Nie, L. V. Saraf, I. A. Aksay, J. Liu and J.-G. Zhang, *Nano Lett.*, 2011, **11**, 5071–5078.
44 B. Sun, P. Munroe and G. X. Wang, *Sci. Rep.*, 2013, **3**, 2247.